JES Focus Issue on Redox Flow Batteries—Reversible Fuel Cells

An Investigation of the Ionic Conductivity and Species Crossover of Lithiated Nafion 117 in Nonaqueous Electrolytes

Liang Su,[a,b] Robert M. Darling,[a,c,*] Kevin G. Gallagher,[a,d,*] Wei Xie,[a,c] Jacob L. Thelen,[a,e] Andres F. Badel,[b] John L. Barton,[a,b] Kevin J. Cheng,[a,f] Nitash P. Balsara,[a,e,*] Jeffrey S. Moore,[a,f] and Fikile R. Brushett[a,b,*,z]

[a] *Joint Center for Energy Storage Research*
[b] *Department of Chemical Engineering, Massachusetts Institute of Technology, Cambridge, Massachusetts 02139, USA*
[c] *United Technologies Research Center, East Hartford, Connecticut 06108, USA*
[d] *Chemical Sciences and Engineering Division, Argonne National Laboratory, Lemont, Illinois 60439, USA*
[e] *Department of Chemical Engineering, University of California, Berkeley, Berkeley, California 94720, USA*
[f] *Department of Chemistry, University of Illinois at Urbana - Champaign, Urbana, Illinois 61801, USA*

Nonaqueous redox flow batteries are a fast-growing area of research and development motivated by the need to develop low-cost energy storage systems. The identification of a highly conductive, yet selective membrane, is of paramount importance to enabling such a technology. Herein, we report the swelling behavior, ionic conductivity, and species crossover of lithiated Nafion 117 membranes immersed in three nonaqueous electrolytes (PC, PC : EC, and DMSO). Our results show that solvent volume fraction within the membrane has the greatest effect on both conductivity and crossover. An approximate linear relationship between diffusive crossover of neutral redox species (ferrocene) and the ionic conductivity of membrane was observed. As a secondary effect, the charge on redox species modifies crossover rates in accordance with Donnan exclusion. The selectivity of membrane is derived mathematically and compared to experimental results reported here. The relatively low selectivity for lithiated Nafion 117 in nonaqueous conditions suggests that new membranes are required for competitive nonaqueous redox flow batteries to be realized. Potential design rules are suggested for the future membrane engineering work.

Manuscript submitted August 26, 2015; revised manuscript received November 18, 2015. Published December 9, 2015. *This paper is part of the JES Focus Issue on Redox Flow Batteries–Reversible Fuel Cells.*

Large scale energy storage for the electricity grid is widely considered to be necessary for enabling the use of intermittent renewables as primary power sources, for stabilizing power delivery in developing economies, and for facilitating a range of high-value grid services aimed at improving efficiency and lifetime.[1] To date, broad market penetration of energy storage systems has been hindered primarily by high installation and operation costs, resulting in only ∼2.5% of the total electricity production in the US relying on grid energy storage predominantly in the form of pumped hydro-electric.[2] However, the rapid and sustained growth of renewable electricity generation (e.g., solar photovoltaic, wind) continues to drive the need for advanced low cost energy storage.[3–5] While certain energy storage technologies, such as lithium-ion (Li-ion) batteries, are currently at a price point to fulfill niche markets,[6] present electrical energy storage technologies, in general, are still not economically viable for wide-scale deployment, spurring research and development efforts worldwide.[7]

Redox flow batteries (RFBs) are electrochemical systems well-suited for multi-hour energy storage and offer several key advantages over enclosed batteries (e.g., Li-ion, Lead-acid) including independent scaling of power and energy, long service life, improved safety, and simplified manufacturing.[8–11] Since their advent in the 1970s,[12] numerous aqueous redox chemistries have been developed but none has experienced widespread commercial success. The use of nonaqueous electrolytes in flow batteries is a nascent, yet burgeoning, concept. Transitioning from aqueous to nonaqueous electrolytes offers an extended window of electrochemical stability (> 3 V) and an enriched selection of redox materials due to the broader design space. However, this approach is not without technical hurdles such as the identification of electrochemical couples with suitably disparate redox potentials, high solubility, and excellent stability. Recent techno-economic analysis by Darling et al. has shown that pathways to meeting the aggressive system cost target (i.e., \$120 kWh^{-1}) exist for both aqueous and nonaqueous RFBs though aqueous systems are at a higher technology readiness level.[13]

Efficient operation of a RFB requires a selective membrane that impedes the crossover of the charge storage molecules while enabling orders of magnitude more facile transport of the ionic charge carrier. Cost-effective flow battery designs require high power density and thus low-impedance membranes so as to minimize the contribution of the reactor to the total system price. The identification of a highly conductive, yet selective membrane is of paramount importance to enabling such a technology. Depending on the chemistry, aqueous RFBs employ either nanoporous (i.e., < 100 nm pores) polyolefin separators or ion-exchange membranes (e.g., Nafion).[14] Thus, despite their higher costs, ion-exchange membranes are typically favored in these batteries due to their high hydraulic resistance and decent proton conductivity. Significant efforts have been focused on developing alternative membranes to replace Nafion in or for aqueous RFBs;[15] however, techno-economic modeling for polymer electrolyte fuel cells (PEFCs) suggests that an order-of-magnitude reduction in Nafion selling price is possible with an increase in the production on scale with the widespread implementation. Approaches to developing new membranes include tailoring membranes to improve a certain key metric (e.g., resistance, crossover) without sacrificing other critical aspects of performance and, in certain cases, employing materials whose poor performance characteristics are offset by their low cost (e.g., non-selective porous separators in Fe-Cr RFBs[16]). As discussed above, nonaqueous RFBs are less mature than their aqueous counterparts and the development of redox chemistries has thus further outpaced the development of separators. The majority of reported nonaqueous RFB active materials focused on positively charged redox species; therefore, anion-exchange membranes have received greater attention to shuttle the counter ions between electrodes.[17] However, the anions used in nonaqueous electrolytes (e.g. PF_6^- or BF_4^-) are the largest cost contributor to the electrolyte and therefore negatively charged redox molecules that associate with inexpensive cations (e.g. Na^+ or Li^+) are seen as the likely path forward for active materials. Thus

*Electrochemical Society Active Member.
[z]E-mail: brushett@mit.edu

Nafion and other cation-exchange membranes are anticipated to receive more interest in nonaqueous RFB development.[13]

High performance separators are required for RFBs, both aqueous and nonaqueous, to meet the aggressive capital cost target. Recently, Darling et al. derived specific transport properties for separators that align with these goals aiming at enabling quantitative analysis of new materials and systems.[18] This work suggests a maximum allowable area-specific resistance (ASR) of 2.3 Ω cm^2 and, in the best case scenario where species crossover does not introduce capacity loss, a maximum allowable crossover current of less than 1% of the discharge current for applicable membranes in nonaqueous RFBs. These performance targets can also be framed in the context of a specific material properties or measurable quantities. For example, the desired ASR corresponds to ionic conductivities of 1.1 mS cm^{-1} and 7.7 mS cm^{-1} for a thickness of 25.4 μm (e.g., Nafion 211) and 177.8 μm (e.g., Nafion 117), respectively. Meanwhile, the maximum allowable crossover current can be quantified as 1.3 mA cm^{-2} based on the ASR targeted operational parameters of a nonaqueous RFB (3.5 V, 130 mA cm^{-2}).

Nafion has been widely used as a cation-exchange membrane. Although the ionic conductivity of Nafion in aqueous environments has been studied for more than two decades,[19] significantly fewer reports about Nafion exist in the context of nonaqueous environments. Here we benchmark the ionic conductivity and species crossover of lithiated Nafion in various nonaqueous electrolytes and compare the measured properties to the target performance metric. Prior reports by Doyle et al. provided foundational guidance on solvent selection and baseline validation for results in the selected solvents.[20] They reported that the ionic conductivity of lithiated Nafion varies over more than five orders of magnitude and correlates this observation to physical properties of solvents. According to Doyle's work, three solvents, propylene carbonate (PC), propylene carbonate : ethylene carbonate (PC : EC), and dimethyl sulfoxide (DMSO), which demonstrated ionic conductivities ranging from 0.01 to 1 mS/cm, are selected in our study. Specifically, we investigate the impact of solvent on the micro-structure of Nafion, and further study the ionic conductivity of lithiated Nafion in $LiPF_6$-based nonaqueous electrolytes with salt concentrations ranging from 0.1 M to 1.5 M. The crossover of redox species was evaluated by measuring the diffusive permeability of neutral, cationic, and anionic model redox species. Through these experimental studies, we aim to develop a relationship between membrane conductivity and active species crossover that, to the best of our knowledge, has not been reported. Such a relationship provides critical design criteria for the development of future practical membrane materials for RFBs.

Experimental

Chemicals.— Propylene carbonate (PC, anhydrous, 99.7%), ethylene carbonate (EC, anhydrous, 99%), dimethyl sulfoxide (DMSO, anhydrous, >99.9%), ferrocene (98%), ferrocenium hexafluorophosphate (97%), and lithium iodide (anhydrous, 99.999%) were purchased from Sigma-Aldrich. Lithium hexafluorophosphate ($LiPF_6$, >99.5%) was purchased from BASF. All chemicals were opened, used, and stored in a positive-pressure, argon (Ar)-filled glove box (Innovative Technology).

Electrolytes.— All solutions were prepared and tested in the glove box. The PC : EC mixed solvent is 1:1 by weight. All solvents / solutions were dried over 3 Å molecular sieve (Sigma-Aldrich) for at least 24 h prior to use. Solution viscosities were measured using a Viscolite 700 viscometer (Vindum Engineering, 0.1 cP resolution). Solution densities were measured by weighing liquid with a known volume on a balance (Mettler-Toledo). Measurements of electrolyte conductivity are described in the membrane conductivity section. All measurements were taken at room temperature (~25°C).

Membrane.— The pristine Nafion 117 membrane (N117, in the protonated form) was purchased from Ion Power. The as-received N117 was pretreated by first boiling the membrane in a bath containing 3% hydrogen peroxide (H_2O_2, Fisher Chemical) for 1 hour. Then the membrane was boiled in 0.25 M sulfuric acid (Sigma-Aldrich) solution for 1 hour and subsequently cleaned in boiling deionized (DI) water (Millipore, 18.2 Ω cm) for 30 min, 3 times. The membrane was then boiled in 0.25 M lithium hydroxide (Sigma-Aldrich) solution for 1 hour and then cleaned in boiling DI water for 30 min, 3 times. Finally, the lithiated N117 membrane (Li-N117) was dried at 120°C under vacuum for 6 days, and then transferred into the glove box without air exposure for storage and subsequent treatment.

Solvent uptake and thickness change.— The membrane dry weight (m_0) and thickness (l_0) were measured by a balance (Mettler-Toledo, 0.1 mg accuracy) and an electronic caliper (Mitutoyo, 0.01 mm accuracy), respectively. For solvent uptake measurements, the dry membranes were equilibrated in the solvent of interest for 3 days and the new weight (m_1) and thickness (l_1) were measured. For electrolyte-equilibrated solvent uptake measurements, the solvent-equilibrated membranes were exposed to an electrolyte (based on the same solvent) for 3 days and the new weight (m_2) and thickness (l_2) were measured again. For all solvent/electrolyte-soaked membranes, residual liquid on the membrane surface was carefully removed using Kimwipes (Kimtech) prior to measurements. 3 days was found to be adequate time for the membranes to equilibrate with the respective electrolytes. The same soaking time was used for protonated N117 in sulfuric acid solution.[21] The solvent weight uptake (ω) is defined as: $\omega = (m_n - m_0)/m_0$, where $n = 1$ or 2. The thickness change (σ) is defined as: $\sigma = (l_n - l_0)/l_0$, where $n = 1$ or 2. All operations were performed in the glove box at room temperature (~25°C). After weight and thickness measurements, the membranes were stored in the corresponding electrolytes, and used for the subsequent conductivity and crossover measurements.

Hydraulic permeability of solvents.— Pure solvent flux was measured using a high-pressure dead-end filtration system (Sterlitech TM HP4750 stirred cell, Sterlitech Co., WA), the schematic illustration of which is shown in Figure 1. The effective mass transfer area of the membrane sample was 14.6 cm^2. Membrane samples were fully saturated in the testing solvent before being transferred into the cell. Pressure was supplied by nitrogen gas and the applied trans-membrane pressure difference was 0.48 MPa gauge. A thermocouple was installed to monitor the temperature of the pressurized solvent, which was 22 ± 0.5°C throughout the test. Permeate was collected and weighed at certain time intervals. According to Darcy's law, the intrinsic hydraulic permeability, k (cm^2), of a porous medium can be calculated from the permeate flow rate, Q (cm^3 s^{-1}), solvent viscosity, μ (Pa s), the membrane thickness, l (cm), the membrane area, A (cm^2), and the applied pressure difference across the membrane, Δp (Pa), as

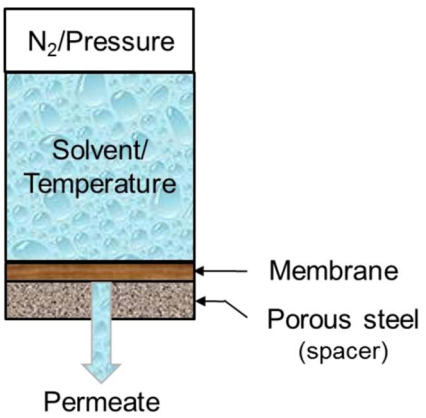

Figure 1. Schematic illustration of the high-pressure dead-end filtration system for solvent hydraulic permeability measurements.

follows:

$$k = \frac{Q\mu l}{A\Delta p} \quad [1]$$

Membrane thickness was measured immediately after a filtration measurement with a thickness gauge (Mitutoyo 389-351 Sheet Metal Micrometer, Mitutoyo).

Membrane conductivity.— The through-plane ionic conductivity of the Li-N117 equilibrated in different electrolytes was measured in a glass H-cell with the membrane mounted between two compartments (James Glass, MA). The same liquid volume (13.5 mL) was maintained in both cell compartments. The electrodes were graphite rods (~10 cm^2 submerged area, McMaster). Cell resistance was measured using a two-electrode configuration via potentiostatic electrochemical impedance spectroscopy (PEIS) controlled by a Bio-Logic VMP3 potentiostat. PEIS was performed from 100 kHz to 100 Hz at an open circuit potential and the high frequency intercept was used to determine cell resistance. The electrolyte conductivity (κ_e, S cm^{-1}) was given by:

$$\kappa_e = \frac{L}{R_1 A} \quad [2]$$

where R_1 is measured cell resistance without a membrane (Ω), L is the electrode-to-electrode distance (6 cm), and A is the cross sectional area of the channel connecting the H-cell compartments (2 cm^2). The membrane conductivity (κ_m, S cm^{-1}) was given by:

$$\kappa_m = \frac{l}{(R_2 - R_1) A} \quad [3]$$

where R_2 is measured cell resistance with a membrane (Ω), l is the membrane thickness after being soaked in the corresponding electrolyte (cm), and A is the cross-sectional area of membrane exposed to the electrolyte (2 cm^2). All operations were performed in the glove box at room temperature (~25°C). Prior to nonaqueous experiments, this methodology was validated using aqueous electrolytes and the results for protonated N117 and Li-N117 were found to be in agreement with published numbers.[20]

Crossover tests of redox species.— Crossover tests were performed in the same H-cell setup (Figure 2). Initially an electrolyte containing 0.05 M redox compound was introduced into one compartment while the same electrolyte without the redox compound was introduced into the other compartment. The two compartments were separated by a membrane that was equilibrated in the same electrolyte prior to testing. The concentration of redox species in each compartment was monitored ex situ every 24 hours via cyclic voltammetry (CV) over a course of 10 days. In detail, 3 mL solution was taken from each side of the H-cell. CV was performed with a three-electrode configuration consisting of a glassy carbon working electrode (GCE, CH Instruments, Inc.), gold coil counter electrode (CH Instruments, Inc.), and fritted lithium (Alfa Aesar) reference electrode containing an electrolyte of 1 M $LiPF_6$/PC : EC (1 : 1 by weight). Automatic *iR* corrections (100%) were applied to all recorded CVs. The changes in peak current on both sides of the H-cell were used to calculate the diffusive permeability of the model redox compounds. All operations were performed in the glove box at room temperature (~25°C). The diffusive permeability (P_0, cm^2 s^{-1}) of the redox active species was calculated according to the following equation for the same volume of solution in both sides:

$$P_0 = \frac{v_B l}{-2At} \ln[1 - 2x_B(t)] \quad [4]$$

where v_B is the electrolyte volume on each side (13.5 cm^3), l is the membrane thickness (cm), A is the membrane area (2 cm^2), t is time (s), $x_B(t)$ is the concentration of crossover species in B side normalized by the initial concentration (0.05 M) in A side. The reported diffusive permeability values reflect the average numbers of the first 3-day measurements (Given the very small value, the diffusivity of I^- in 1 M $LiPF_6$/PC is an average number of the last 3-day measurement). Equation 4 was derived from the commonly used diffusive permeability calculation from literature[17,22] considering the concentration change of active species in both sides.

Diffusivity of redox species.— The diffusivity of the redox species was estimated using the Randles-Sevcik equation:

$$j_p = 0.4463nFC_{A,b}\sqrt{\frac{nF\upsilon D_0}{RT}} \quad [5]$$

where j_p is the peak current density (A cm^{-2}), which is the peak current normalized by the geometric area of the glassy carbon electrode (0.071 cm^2), n is the number of electrons transferred in the redox event, F is Faraday's constant (96,485 C mol^{-1}), $C_{A,b}$ is the bulk concentration of active species (mol cm^{-3}), υ is the scan rate (V s^{-1}), D_0 is the diffusivity (cm^2 s^{-1}), R is the universal constant (8.314 J mol^{-1} K^{-1}), and T is the absolute temperature (K). The anodic peak currents were used for Fc and I^- and the cathodic peak current were used for Fc^+. The bulk concentrations of the active species were all 5×10^{-5} mol cm^{-3}. Scan rates for all measurements were 0.02 V s^{-1}.

Small angle x-ray scattering.— Synchrotron small- and wide-angle X-ray scattering (SAXS / WAXS) were performed at the Advanced Light Source, Beamline 7.3.3 at Lawrence Berkeley National Laboratory[23] to probe the microstructure of the Li-N117. The sample-to-detector distance and beam center were calibrated using a silver behenate standard. Scattering was performed in transmission geometry using a custom-built hermetically sealed sample holder (Figure 3). A blank sample consisting of pure solvent (argon gas) was prepared for each measurement. The 2D scattering patterns were azimuthally integrated using the Nika macro developed by Jan Ilavsky[24] to yield 1D data sets of intensity (I) versus the magnitude of the scattering vector:

$$q = \frac{4\pi}{\lambda_w} \sin\left(\frac{\theta}{2}\right) \quad [6]$$

where λ_w is the radiation wavelength (nm) and θ is the scattering angle (degree) as depicted in Figure 3. Reduced SAXS data were further processed by subtracting the background scattering from the corresponding blank sample and calibrated to a glassy carbon absolute intensity standard (sample M13, Jan Ilavsky).[25] Intensity error estimates calculated by the Nika macro were propagated through the calibration procedure assuming random error statistics. Calibrated scattering intensity from 2D data collected at different sample-to-detector

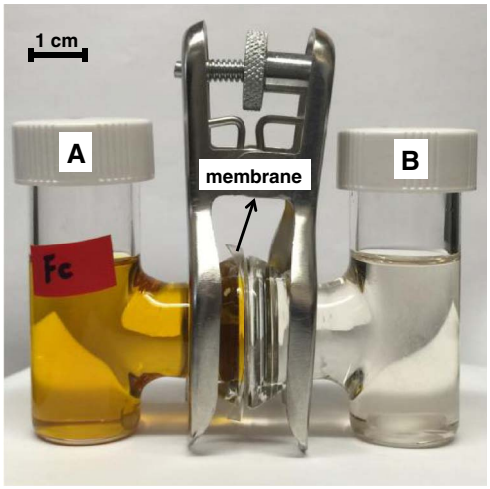

Figure 2. Digital photograph of the H-cell setup used for both membrane conductivity and crossover tests. The H-cell is shown in crossover test mode with left compartment containing Fc. During operation, this cell would be placed on a magnetic stir plate an Ar-filled glove box.

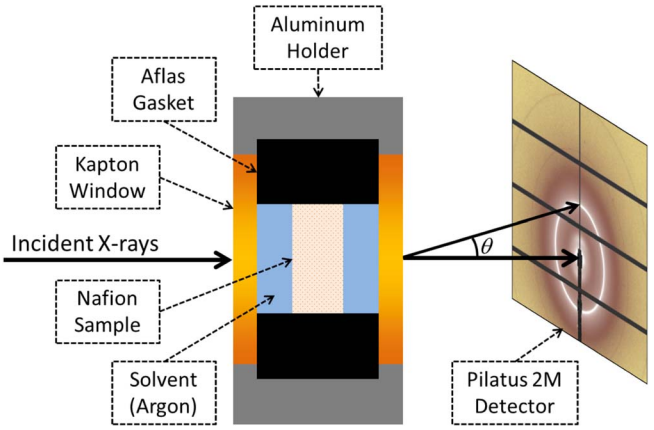

Figure 3. Schematic of the scattering measurement geometry and sample holder design.

distances overlay well and allow us to extend the q- range probed ($q = 0.04$–3.0 nm^{-1}).

Results and Discussion

Solvent uptake and microstructure of Li-N117 in nonaqueous solvents.— We report here some macroscopic and microscopic changes due to the swelling of Li-N117 in nonaqueous environments. The ionic conductivity, viscosity, and density of the electrolytes are provided in the appendix (Tables AI–AIII). The conductivity and viscosity numbers in PC-based electrolytes are in agreement with literature.[26] The weight uptakes of Li-N117 equilibrated in the pure solvents are shown in Table I and compared with the values reported by Doyle et al.[20] The trends in weight uptake are in good agreement with the prior report; however, uniformly lower solvent uptake values (ca. 10–20%) were observed. These variations might be attributed to the differences in membrane preparation procedures. To ensure that this was not an artifact of incomplete equilibration, weight uptakes were measured after soaking the membranes in each solvent for 1, 2, and 3 days. Experimental results show that the weight uptakes of the Li-N117 reach equilibrium after 1 day of soaking although all data reported here are from the membranes after 3 days of soaking.

The increased weight of the membrane is the result of solvent absorption, which primarily depends on the solvent donor number.[27] The size of Li-N117 increases in all 3 dimensions upon solvent uptake. However, the swelling of membrane is anisotropic favoring the direction along thickness, which is likely due to the much smaller through-plane dimension (~0.018 cm) than the in-plane dimensions (~2.5 cm × 2.5 cm).[27] From the macroscopic solvent weight uptake, we can calculate the solvent molar uptake (λ) and the solvent volume fraction (Φ) of Li-N117. Solvent molar uptake reflects the molar ratio of Li^+ and solvent molecules within the membrane. For a given solvent, solvent molar uptake in the membrane can be calculated as:

$$\lambda = \frac{\omega}{M_0} EW \quad [7]$$

where ω is the weight uptake, M_0 is the molecular weight of the solvent (g mol^{-1}), and EW is the equivalent weight of the perfluorosulfonated ionomer. For N117, $EW \approx 1100$ g mol^{-1}. The solvent volume fraction might be visualized as the content of the solvent-wettable domain in the membrane. For a given solvent, solvent volume fraction in the membrane can be calculated as:

$$\Phi = \frac{\lambda V_{solvent}}{\lambda V_{solvent} + V_{Nafion}} = \frac{\lambda M_0/\rho_0}{\lambda M_0/\rho_0 + EW/\rho_{Nafion}} \quad [8]$$

where λ is the solvent molar uptake, $V_{solvent}$ is the solvent molar volume (cm^3 mol^{-1}), V_{Nafion} is the molar volume of the perfluorosulfonated polymer of Nafion (cm^3 mol^{-1}), ρ_0 is the solvent density (g cm^{-3}), ρ_{Nafion} is the density of perfluorosulfonated polymer of Nafion, which is approximated as 2.1 g cm^{-3} according to the literature.[21,28] Ideal solution approximation was applied in the derivation of Equation 8 at all concentrations of $LiPF_6$ in the electrolyte. Based on the solvent volume fraction, the effective pore diameter (d, cm) of the solvent-swollen Li-N117 can be estimated according to a pseudo 3D capillaric model:[29]

$$d = \sqrt{\frac{96k}{\Phi}} \quad [9]$$

where k is the hydraulic permeability of solvent (cm^2) and Φ is the solvent volume fraction.

Table I summarizes the solvent molar uptake, solvent volume fraction, and the calculated pore size of Li-N117 in PC, PC : EC, and DMSO. The effective pore size of Li-N117 in PC is 0.52 nm. The presence of EC, which is a commonly used co-solvent in Li-ion batteries,[30] increases the number to 0.78 nm. A larger pore size of 2.08 nm was observed when soaking the membrane in DMSO. The solvent molar uptake and the hydraulic permeability for protonated N115 in water were experimentally determined as 21 and 3.75×10^{-16} cm^2, respectively, at 23°C according to Duan et al.[31] These numbers lead to a pore size of 2.93 nm for protonated N115 in water based on 3D capillaric model. In comparison, the pore diameters of protonated N117 in aqueous system typically range from ~1 to 3 nm based on different theoretical calculations.[32]

The trend of the microstructural impact of membrane swelling in different solvents can be further verified by small-angle X-ray scattering. As shown in Figure 4, the scattering patterns for Li-N117 generally contain two features. The feature at higher q corresponds to the "ionomer peak", which results from the scattering between clusters of the sulfonic groups (RSO_3^-) and the swelling solvent.[19,33–35] The feature at lower q, typically labeled as the Nafion "matrix knee" where the scattered intensity is caused by crystallites of the fluorocarbon polymer backbone randomly distributed in an amorphous polymer matrix.[19,33,34] The position of ionomer peak appears to be insensitive to the identity of the swelling solvent. On the other hand, the position of matrix knee systematically shifts to decreased q values with the increase of solvent uptake. Note that the dry Li-N117 sample only demonstrates the "matrix knee", consistent with previous study.[34] The characteristic distance between adjacent ion-containing channels (d_i) in the swollen polymers is related to the location of the ionomer peak (q_i):

$$d_i = \frac{2\pi}{q_i} \quad [10]$$

The values of d_i obtained by SAXS are 6.3 ± 1.5 nm, 6.1 ± 0.2 nm, and 6.2 ± 0.8 nm for PC, EC : PC, and DMSO samples, respectively. Estimates of pore sizes based on SAXS require the knowledge of solvent distribution in the ionic and nonionic domains, which is currently unavailable. Qualitatively, one may expect the characteristic distance between crystallites to increase due to swelling. The characteristic distances between the crystallites (d_c) can be obtained

Table I. Membrane swelling of Li-N117 in pure solvents: PC, PC : EC, and DMSO. The values in brackets are from Ref. 20. The asterisk on the PC : EC data denotes a 1:1 by volume mixture was used in literature[20] whereas a 1:1 by weight mixture was used in this work. The standard errors reflect measurements from 3 independent membranes.

Solvent	Weight uptake (%)	Molar uptake	Volume fraction (%)	d (nm)
PC	54.8 ± 0.2 [65]	5.9 ± 0.1	48.9 ± 0.1	0.52
PC : EC	60.3 ± 0.2 [85*]	7.0 ± 0.1	49.9 ± 0.1	0.78
DMSO	124.7 ± 0.4 [136]	17.6 ± 0.1	70.5 ± 0.1	2.08

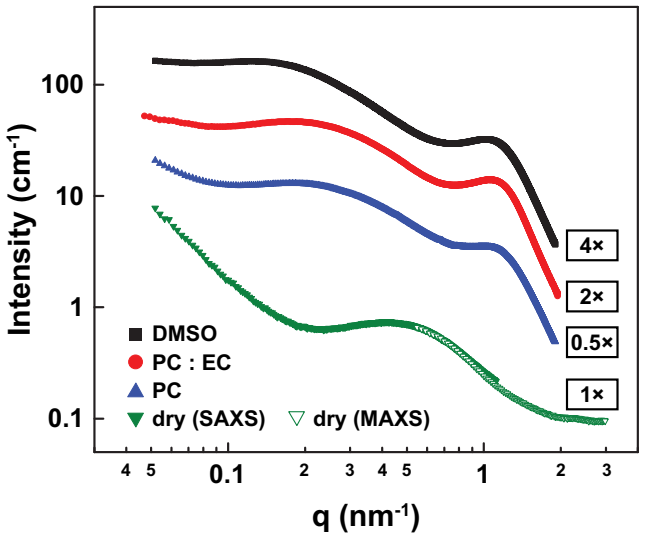

Figure 4. Absolute SAXS intensity profiles for Li-N117 equilibrated in DMSO, PC : EC, PC, as well as the dry membrane. The solid shapes represent data collected with a large detector distance (c.a. 4 m) and the open triangles for the dry membrane represent data collected with a short detector distance (c.a. 0.3 m), both of which were independently calibrated to yield the portrayed scattering profiles. For clarity, the DMSO, PC : EC, and PC data were multiplied by a factor of 4, 2, and 0.5, respectively, and the intensity error estimates were omitted.

from the location of the matrix knee (q_m):

$$d_c = \frac{2\pi}{q_m} \quad [11]$$

In dry Nafion, $d_{c,dry} = 14.8 \pm 4.5$ nm, while in the swollen samples, d_c values have been determined to be 34.5 ± 6.0 nm, 36.5 ± 3.4 nm, and 53.3 ± 18.9 nm for PC, PC : EC, and DMSO. Compared to that of dry Li-N117, the increased d_c values result from the membrane swelling in these solvents. The trend of d_c values determined by SAXS is consistent with that of the effective pore size determined by solvent uptake and hydraulic permeability. Please note the there is more than an order of magnitude difference between d_c and the hydraulic permeability derived pore size (d) of Li-N117. The effective size of the pore and the distance between crystallites are related, but not with the same characteristic length. A mathematical expression to connect these two characteristic lengths relies upon an assumed physical model of the membrane and requires knowledge of the microscopic solvent distribution that is unknown at this time.

Swelling and conductivity of Li-N117 in nonaqueous electrolytes.— The working solutions in RFBs consist of active species dissolved in an electrolyte that contains a certain amount of supporting salt to enhance the ionic conductivity and to provide counter-ions for the electrode reactions. Therefore, the swelling properties of Li-N117 were also investigated in electrolytes containing $LiPF_6$ at different concentrations. As shown in Figure 5a, the solvent volume fraction in Li-N117 decreases with the increase of salt concentration, which also results in the decrease of the macroscopic dimensions of the membrane. The equilibration process for a dry membrane soaking in pure solvent has been described by Doyle et al.[20] Qualitatively, solvent molecules initially enter the membrane to solvate the Li^+ bound with the anionic sites on the polymer backbone. Afterwards, solvent transport continues into the membrane to decrease the Li^+ concentration in the membrane. At a certain swelling state, the elasticity of the membrane prevents further solvent uptake where the chemical potential difference of solvent (or salt) inside and outside the membrane reaches equilibrium with the strain on the membrane. When placing the solvent-soaked membrane in the electrolyte, solvent molecules tend to diffuse out of the membrane to lower the chemical potential of solvent in the electrolyte and meanwhile to decrease the strain on the membrane. Therefore, concentrated electrolytes tend to result in less solvent uptake in the membrane. A lower volume fraction of solvent in the membrane leads to a reduced overall membrane porosity and a decreased characteristic pore size. Similar pore size constriction has been observed for the protonated N117 with the increase of sulfuric acid concentration in aqueous system.[21]

Figure 5b presents the through-plane ionic conductivity (κ_m) of Li-N117 in various electrolytes. At the same $LiPF_6$ concentration, the order of κ_m always follows: PC < PC : EC < DMSO, which is consistent with that of the in-plane conductivities of Li-N117 in the same set of pure solvents.[20] The change of κ_m of Li-N117 with increasing $LiPF_6$ concentration is solvent dependent. For PC-based electrolytes, higher salt concentration results in a monotonic decrease of κ_m. We hypothesize that this decrease is largely due to the constriction of pores in the membrane. As estimated via solvent hydraulic permeability analysis, the effective pore size of PC-soaked Li-N117 is ~0.53 nm, which is even smaller the diameter of solvated Li^+ in PC (~0.88 nm[26]). Higher salt concentration in the electrolyte results in the reduced pore size in the Li-N117, thus further slowing charge transport through the membrane. The decrease in membrane conductivity is counter to the increase in electrolyte conductivity (κ_e) with increasing $LiPF_6$ concentration (Table AI). In addition to the decreased pore size, the loss of solvent in the membrane can lead to changes in the interactions between mobile cations (Li^+) and the fixed anions (RSO_3^-), which may adversely impact the membrane conductivity as well.[36] A similar trend was observed in the case of PC : EC-based electrolytes although

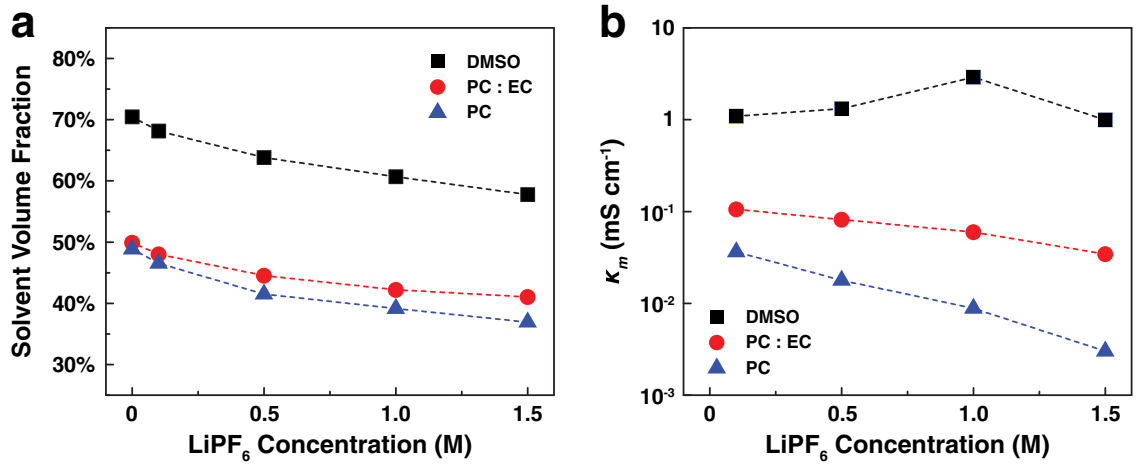

Figure 5. (a) The solvent volume fraction and (b) membrane conductivity as a function of $LiPF_6$ concentration in the external electrolyte. Each data point reflects an average of measurements from 3 independent membranes. The error bars ranging from 0.1–0.3% for (a) and 2.9–8.5% for (b) are too small to be resolved here.

κ_m decreases slower with increasing salt concentration, which may be due to a larger initial solvent volume fraction in the membrane. Nevertheless, in both cases, κ_m is at least 18× lower than the target membrane conductivity value (1.1 mS cm^{-1}), which eliminates the possibility of using these membrane-electrolyte combinations for nonaqueous RFBs. In contrast, high ionic conductivity ($\geq$ 1 mS cm^{-1}) can be obtained in DMSO-based electrolytes. Furthermore, in DMSO, both membrane and electrolyte conductivities increase with increasing salt concentration until 1 M $LiPF_6$ and decrease thereafter. This observation suggests that, although the solvent volume fraction in the membrane still decreases with increasing salt concentration in the surrounding electrolyte, the pore diameter is expected to be much larger than the diameter of the solvated Li^+ in DMSO and may allow for $LiPF_6$ to imbibe in the membrane. Consequently, the ionic conductivity of the membrane can be approximated as:[37]

$$\kappa_m = \kappa_e \varepsilon^n \quad [12]$$

where ε is the porosity and n is a function of structural properties of the separator (porosity, tortuosity, etc.). Thus, the trend of κ_m should be in line with that of κ_e as long as the pore size is not a limiting factor for the mass transfer of Li^+. The increased κ_e dominates the decreased ε at higher salt concentration in DMSO. More rigorous quantitative analysis on the relationship between the solvated ion size and the membrane pore size is on-going and will be reported in due course. Compared to that in carbonated-based electrolyte, the higher membrane conductivity in DMSO-based electrolyte might also, at least partially, be attributed to higher charge carrier (Li^+) dissociation from the tethered RSO_3^- group in DSMO.[38] Note that even in the best-case scenario here (1 M $LiPF_6$ / DMSO), the ionic conductivity of Li-N117 is still significantly lower than that of the same membrane in an aqueous environment (16 mS cm^{-1}, in-plane conductivity[20]).

Crossover of active species.— Besides the conductivity requirement, a successful membrane for nonaqueous RFBs should also be able to minimize the crossover of active species. Recently, lithiated perfluorinated ionomer has been used as a cation-exchange membrane in a nonaqueous RFB[39] and lithium ion battery.[40] However, the "ion selective" mechanism of these membranes has yet to be demystified. A tempting hypothesis in this regard is the negatively charged RSO_3^- group fixed on the polymeric backbone promoting the transport of positively charged species and meanwhile, retarding the transport of negatively charged species. Herein, we investigated the diffusive property of redox species across Li-N117 in nonaqueous electrolytes. Specifically, ferrocenium hexafluorophosphate ($Fc^+PF_6^-$), ferrocene (Fc), and lithium iodide (Li^+I^-) were selected as the model redox compounds with positive, neutral, and negative charge, respectively. Two different $LiPF_6$ concentrations, 0.1 M and 1 M, were used in each solvent. Only Fc and LiI were tested in DMSO-based electrolytes since Fc^+ is not chemically compatible with DMSO.

Mass transfer resistance of the active species.—The total mass transfer resistance of the active species traveling across the membrane (R_{mt}, s cm^{-1}) reflects the intrinsic diffusive resistance of the active species ($R_{mt,d}$) plus the additional mass transfer resistance of the active species due to the interaction between the active species and the membrane ($R_{mt,m}$):

$$R_{mt} = R_{mt,d} + R_{mt,m} \quad [13]$$

To study the interaction between the active species and the membrane, it is important to deconvolute $R_{mt,m}$ from R_{mt}:

$$R_{mt,m} = R_{mt} - R_{mt,d} \approx l\left(\frac{1}{P_0} - \frac{1}{D_0}\right) \quad [14]$$

where R_{mt} is expressed as the membrane thickness (l) times the reciprocal of permeability (P_0) and $R_{mt,d}$ is expressed as the membrane thickness (l) times the reciprocal of diffusivity (D_0). The diffusivity of the active species within the membrane is approximated as that in the bulk solution at a certain salt concentration.

The experimental data in terms of the species concentration change with time are presented in Figures 6a, 6b, 6c, and the $R_{mt,m}$ numbers are presented in Figure 6d. The corresponding permeability and diffusivity numbers are summarized in the Appendix (Table AIV). Major trends throughout all the combinations of salt concentration, solvent, and redox molecule include: 1) for the same redox species and solvent, higher salt concentration results in lower crossover; 2) for the same concentrations of salt and redox species, the crossover rate follows PC < PC : EC < DMSO; 3) for the same electrolyte (certain concentration of salt + solvent), the crossover rate follows $I^- < Fc < Fc^+$.

The size effect and the charge effect are generally believed as the governing factors for the diffusion of active species across an "ion-selective membrane". The size selectivity, which is also known as steric hindrance, of a membrane affects the mass transfer of molecules / ions by the difference between the size of pores and the solvated diameter of the crossover species.[41] The charge selectivity of Li-N117, according to the principle of Donnan exclusion,[42] functions such that the negative charged RSO_3^- group attracts counter-ions and repels co-ions, and thus facilitates the mass transfer of cations and retards that of anions.

Size effect.—In line with Figure 5a, the increase of salt concentration (*trend 1*) or the change of solvent from DMSO to PC : EC to PC (*trend 2*) reduces the solvent volume fraction in Li-N117, and consequently, constricts pores of the membrane, which results in larger mass transfer resistance, and experimentally, lower crossover rate of the redox active species. The selection of separator should consider the size of redox active molecules. For example, the DMSO-soaked Li-N117 used here has an effective pore diameter smaller than 2 nm; however this electrolyte-membrane combination has little crossover resistance of either neutral or negatively charged molecules. Therefore, it seems that a RFB using smaller redox active compounds (MW < 200) necessitates the separator with pores or linkages between pores in the reverse-osmosis or nanofiltration size range.[18]

Charge effect.—Neutral molecules (no charge) should not be biased by the tethered ions in an ion-exchange membrane, which makes Fc a good reference point in the discussion here. The "charge selectivity" of the cation-exchange Li-N117 promotes the mass transfer of Fc^+ across the membrane in comparison with that of Fc. Therefore, if we assume that the sizes of Fc^+ and Fc are close according to their similar diffusivities in the solution (Table AIV), the mass transfer resistance of Fc^+ across the membrane should be lower than that of Fc in any electrolyte, which has been validated in Figure 6d. It is worth mentioning that the difference of mass transfer resistance between Fc and Fc^+ decreases with the increase of salt concentration, which indicates that the electrolyte with higher ionic strength seems to diminish the charge selectivity of membrane. This observation is in agreement with the Donnan exclusion calculations from our previous work.[18] Higher salt concentration is required in redox flow batteries to ensure high conductivity of the electrolyte. Therefore, the applicability of a "charge-selective membrane" in such a working condition would be questionable. A crude analysis from the diffusive permeability results also shows that the mass transfer resistance of I^- traveling across the membrane is much larger than that of Fc, which also seems to be consistent with the charge selectivity argument. However, due to the lack of the size information of the solvated I^- in these electrolytes, we would be hesitant here to make such a conclusion. Computational effort using molecular dynamics (MD) for the calculation of solvated ions is underway.

Relationship between membrane conductivity and species crossover.— In a RFB, we would like to maximize the coulombic efficiency and the voltage efficiency by decreasing the species crossover and increasing the membrane conductivity, respectively. Therefore, regardless of the interaction between the membrane and the redox species ($R_{x,m}$), it is of particular interest from a practical RFB operation standpoint to understand the relationship between the membrane conductivity and the species crossover. To this end, we define the

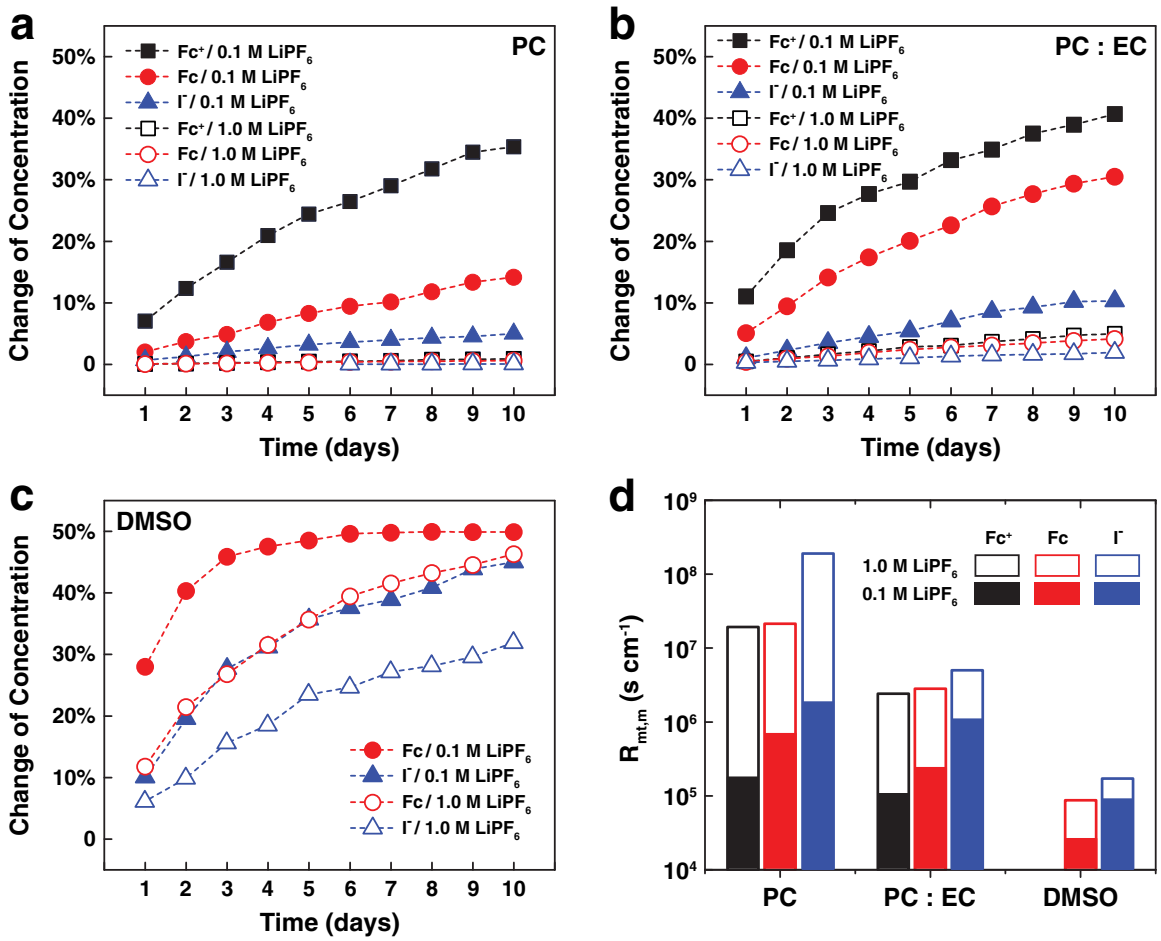

Figure 6. The crossover of Fc^+ (square), Fc (circle), and I^- (triangle) as a function of time in (a) PC-, (b) PC : EC-, and (c) DMSO- based electrolytes containing 0.1 M (solid) and 1.0 M (open) $LiPF_6$ as the supporting salt. (d) The mass transfer resistance of the redox species from the membrane in each solution condition.

dimensionless selectivity (α) of the membrane as:

$$\alpha \equiv \frac{R_x}{R_m} \quad [15]$$

where R_x is the overall area-specific ohmic resistance of the membrane to the crossover of active species ($\Omega\ cm^2$) and R_m is the area-specific ohmic resistance of the membrane to the crossover of charge carriers ($\Omega\ cm^2$). R_x can be further expressed using an analogy of Ohm's law as:

$$R_x = \frac{RT}{i_x F} \quad [16]$$

where i_x is the crossover current of the active species and can be further formulated as:[43]

$$i_x = \phi \frac{F}{A} \frac{dn_A(t)}{dt} = \frac{\phi F P_0 \Delta C_b}{l} \approx \frac{\phi F P_0 C_{A,b}}{l} \quad [17]$$

ϕ is the dimensionless proportionality constant that depends on the number of electrons associated with the crossover species. We take ϕ = 1 in this work. F is the Faraday constant (96,485 C mol^{-1}); A is the area (cm^2); $dn_A(t)\ /\ dt$ is the crossover rate of active species (mol s^{-1}); P_0 is the diffusive permeability ($cm^2\ s^{-1}$); ΔC_b is the bulk concentration difference of active species across the membrane (mol cm^{-3}), which can also be deemed as the driving force of the diffusive crossover of active species; l is the thickness of the membrane. The second approximation applies if we assume that the amount of active species going across the membrane is much smaller than that of the original active species in the bulk solution ($n_{A,x} \ll n_{A,b}$). R_m can be expressed as:

$$R_m = \frac{l}{\kappa_m} \quad [18]$$

where κ_m is the membrane conductivity (S cm^{-1}) and l is the membrane thickness (cm). Therefore, combining Equations 15 to 18, α can be expressed as:

$$\alpha = \frac{RT}{F^2 C_{A,b}} \frac{\kappa_m}{P_0} \quad [19]$$

To study the selectivity of the membrane in different electrolytes, we plot the conductivity of Li-N117 versus the diffusive permeability of Fc in Figure 7. One can see that at a given salt concentration, the membrane conductivity increases almost linearly with increasing the species permeability, indicating that simultaneously obtaining high conductivity of the membrane and low crossover of the active species seems to be unlikely. On the other hand, increasing salt concentration leads to higher selectivity for this Li^+–Fc system. However, we cannot rule out the possibility that the larger crossover at lower salt concentration might be due to the larger solvent activity difference across the H-cell. Furthermore, the presence of flowing solution, electrical field, and high-concentration redox active compounds could adversely affect the selectivity of the membrane. Therefore, future work along this direction should be focusing on a system-level crossover tests for a certain membrane-redox couple-electrolyte combination under the real operation condition of nonaqueous RFBs. It can also be seen from Figure 7 that even at the static cell condition at low concentration of redox active species, none of the membrane/electrolyte combinations here hit the target performance metric, which signifies the urgency for developing functional separator and/or redox active materials to enable an economically viable nonaqueous RFBs.

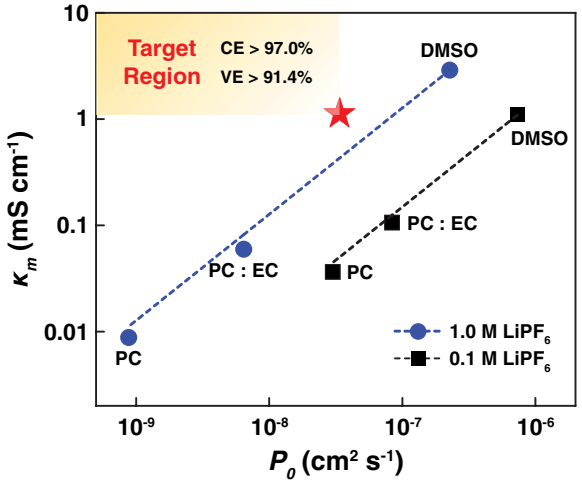

Figure 7. The conductivity of Li-N117 as a function of the permeability of Fc. The conductivity values are obtained from Figure 5b and the diffusive permeability numbers are obtained from Table AIV. The star is the target membrane conductivity (1.1 mS cm^{-1} with a thickness of 25.4 μm) and target species permeability (3.42 × 10^{-8} cm^2 s^{-1}) for a nonaqueous RFB with an open circuit voltage at 3.5 V operated at 130 mA cm^{-2}, 1 M redox active species, and at 25°C. The target region as well as the coulombic efficiency (CE) and voltage efficiency (VE) numbers is also in line with this operating condition.

Linking selectivity to flow cell efficiency.— The maximum energy efficiency of a RFB can be quantitatively linked to the selectivity of the membrane with a simple model provided a number of assumptions are permitted:

$$\varepsilon_{e,rt} = \left[1 - \sqrt{\frac{\phi\,(1+\tau)\left(1+\tau^{-1}\right)RT}{\alpha U F}}\right]^2 \qquad [20]$$

where $\varepsilon_{e,rt}$ is the maximum round-trip energy efficiency, ϕ is the dimensionless proportionality constant, τ is the ratio of charge time to discharge time, U is the open circuit voltage (V), and α is the selectivity. Detailed derivation of Equation 20 along with relevant assumptions can be found in one of our recent publications.[43]

Figure 8 shows the required minimum selectivity as a function of energy efficiency for $U = 1.25$ V and $U = 3.5$ V at $T = 25$°C and $\tau = 2$. The lower U represents aqueous RFBs such as a vanadium redox flow battery, while the higher U represents nonaqueous RFBs

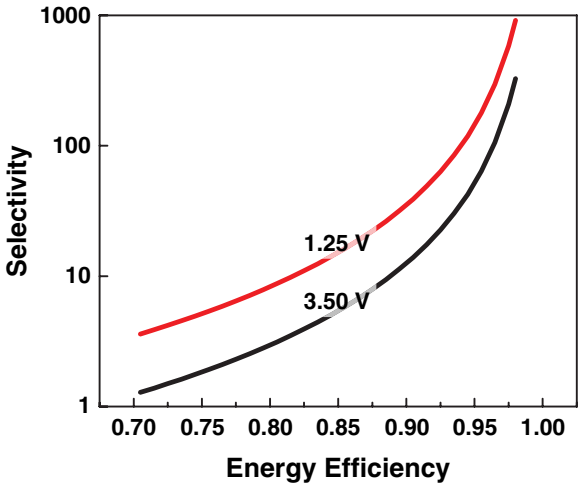

Figure 8. Minimum required selectivity as a function of the maximum energy efficiency for RFBs with an open circuit voltage of 1.25 V (aqueous) and 3.5 V (nonaqueous).

such as those contemplated in this work. Since the required selectivity is a strong function of efficiency, the selectivity is represented on a log scale while the energy efficiency is on a linear scale. Required selectivity increases with decreasing OCV. To reach the same energy efficiency, the membrane selectivity requirement in the context of nonaqueous RFBs is less stringent that that for aqueous RFBs, which could potentially decrease the capital cost of the reactor.

Conclusions and Recommendations

The process of deriving performance requirements[18] and evaluating commercially available materials has led to the identification of high-level design rules for membranes that would enable nonaqueous RFBs. This work reports important performance characteristics in terms of the conductivity of membrane and the permeability of redox active species for Li-N117 in PC-, PC : EC- and DMSO-based electrolytes in the context of nonaqueous RFB applications. The experimental data presented herein indicates that dramatic differences in membrane conductivity in nonaqueous solvents may be primarily linked to the solvent volume fraction and the degree of charge carrier dissociation from the tethered ion. Intuitively, a larger solvent volume fraction within the membrane typically means increased pore sizes and the overall porosity which, in turn, facilitates higher mass transfer of ions and/or molecules, thus simultaneously increasing membrane conductivity and crossover of redox species. Quantitatively, a linear relationship between the diffusive crossover of ferrocene and the conductivity of Li-N117 was identified, both of which are dominated by the size difference between the pores and the transferring ions. Further, charge exclusion is found to be active but less important than size exclusion, especially in highly concentrated electrolytes, which is in agreement with Donnan exclusion calculations reported elsewhere.[18] However, the relatively low conductivities or selectivities of Nafion under nonaqueous conditions suggest that new membranes are required before a competitive nonaqueous RFB could be implemented.

A membrane synthesized via molecular engineering to achieve both high conductivity and high selectivity should possess three traits: 1) domains of low tortuosity to enable facile conduction, 2) small transport lengths between high conduction domains that impart selectivity, 3) the selection of appropriate solvent to dissociate co-ion from the tethered ion and 4) a size-screening pore size should be sufficiently larger (at least 2×) than that of the solubilized counter-ion required for conduction, leading to high voltage efficiency, meanwhile smaller than that of the active species to enable selectivity of active molecule, contributing to high coulombic efficiency.

Acknowledgments

This work was supported as part of the Joint Center for Energy Storage Research, an Energy Innovation Hub funded by the U.S. Department of Energy, Office of Science, Basic Energy Sciences. Beamline 7.3.3 of the Advanced Light Source is supported by the Director of the Office of Science, Office of Basic Energy Sciences, of the U.S. Department of Energy under Contract No. DE-AC02-05CH11231.

Appendix

Table AI. Viscosity, density, and ionic conductivity of PC with varying $LiPF_6$ concentrations.

[$LiPF_6$] (mol L^{-1})	Viscosity (cP)	Density (g mL^{-1})	Conductivity (mS cm^{-1})
0.0	2.57	1.20	–
0.1	2.80	1.21	2.02
0.5	4.37	1.25	5.78
1.0	8.42	1.29	6.07
1.5	18.00	1.33	4.57

Table AII. Viscosity, density, and ionic conductivity of PC : EC with varying $LiPF_6$ concentrations.

[$LiPF_6$] (mol L^{-1})	Viscosity (cP)	Density (g mL^{-1})	Conductivity (mS cm^{-1})
0.0	2.53	1.27	–
0.1	2.74	1.28	2.06
0.5	4.10	1.31	6.44
1.0	7.35	1.35	7.33
1.5	14.47	1.39	5.78

Table AIII. Viscosity, density, and ionic conductivity of DMSO with varying $LiPF_6$ concentrations.

[$LiPF_6$] (mol L^{-1})	Viscosity (cP)	Density (g mL^{-1})	Conductivity (mS cm^{-1})
0.0	2.00	1.10	–
0.1	2.16	1.11	2.68
0.5	2.86	1.14	8.88
1.0	4.45	1.19	10.82
1.5	7.72	1.23	9.13

Table AIV. Permeability and diffusivity of active species in different electrolytes.

Solvent	[$LiPF_6$] (mol L^{-1})	Active materials	Permeability (cm^2 s^{-1})	Diffusivity (cm^2 s^{-1})
PC	0.1	Fc^+	1.120E-07	2.319E-06
PC	0.1	Fc	3.002E-08	2.400E-06
PC	0.1	I^-	1.067E-08	6.145E-07
PC : EC	0.1	Fc^+	1.826E-07	2.447E-06
PC : EC	0.1	Fc	8.356E-08	2.406E-06
PC : EC	0.1	I^-	1.788E-08	9.017E-07
DMSO	0.1	Fc^+	–	–
DMSO	0.1	Fc	7.306E-07	3.833E-06
DMSO	0.1	I^-	2.188E-07	1.688E-06
PC	1.0	Fc^+	9.782E-10	8.113E-07
PC	1.0	Fc	8.824E-10	1.135E-06
PC	1.0	I^-	1.027E-10	1.756E-07
PC : EC	1.0	Fc^+	7.506E-09	1.077E-06
PC : EC	1.0	Fc	6.448E-09	1.450E-06
PC : EC	1.0	I^-	3.689E-09	1.726E-07
DMSO	1.0	Fc^+	–	–
DMSO	1.0	Fc	2.280E-07	2.701E-06
DMSO	1.0	I^-	1.030E-07	4.763E-07

List of Symbols

A	area (cm^2)
C	concentration of active species (mol cm^{-3})
D_0	diffusivity (cm^2 s^{-1})
EW	equivalent weight (g mol^{-1})
F	Faraday constant (96,485 C mol^{-1})
L	electrode-to-electrode distance (cm)
M	molecular weight (g mol^{-1})
P_0	diffusive permeability (cm^2 s^{-1})
Q	flow rate (cm^3 s^{-1})
R	ideal gas constant (8.314 J mol^{-1} K^{-1})
R_m	area-specific ohmic resistance of the membrane (Ω cm^2)
R_{mt}	total mass transfer resistance (s cm^{-1})
$R_{mt,d}$	diffusion mass transfer resistance (s cm^{-1})
$R_{mt,m}$	membrane mass transfer resistance (s cm^{-1})
R_n	resistance of H-cell (Ω)
R_x	area-specific ohmic resistance of the species crossover (Ω cm^2)
T	temperature (K)
U	open circuit voltage (V)
V	molar volume (cm^3 mol^{-1})
d	effective diameter of the pore (cm)
d_c	characteristic distance of crystallites (nm)
d_i	characteristic distance between adjacent ion-containing channels (nm)
i_x	crossover current density (A cm^{-2})
j_p	peak current density (A cm^{-2})
k	hydraulic permeability (cm^2)
l	thickness of membrane (cm)
m	weight of membrane (g)
n	number of electron transfer (–)
q_i	position of the ionomer peak (nm^{-1})
q_m	position of the matrix knee (nm^{-1})
t	time (s)
v	volume of electrolyte (cm^3)
x	normalized concentration of crossover species (–)

Greek

Δp	pressure difference (Pa)
Φ	solvent volume fraction (–)
ϕ	proportionality constant (–)
α	membrane selectivity (–)
ε	membrane porosity (–)
$\varepsilon_{e,rt}$	round-trip energy efficiency (–)
θ	scattering angle (°)
κ_e	electrolyte conductivity (S cm^{-1})
κ_m	membrane conductivity (S cm^{-1})
λ	solvent molar uptake (–)
λ_w	radiation wavelength (nm)
μ	viscosity (Pa s)
υ	scan rate (V s^{-1})
ρ	density (g cm^{-3})
τ	ratio of charge time to discharge time (–)
ω	solvent weight uptake (–)

References

1. A. A. Akhil, G. Huff, A. B. Currier, B. C. Kaun, D. M. Rastler, S. B. Chen, A. L. Cotter, D. T. Bradshaw, and W. D. Gauntlett, DOE/EPRI 2013 electricity storage handbook in collaboration with NRECA. Sandia National Laboratories (2013).
2. Electric Power Research Institute, DOE handbook of energy storage for transmission and distribution applications (2003).
3. S. Chu and A. Majumdar, *Nature*, **488**, 294 (2012).
4. B. Dunn, H. Kamath, and J.-M. Tarascon, *Science*, **334**, 928 (2011).
5. Z. Yang, J. Zhang, M. C. W. Kintner-Meyer, X. Lu, D. Choi, J. P. Lemmon, and J. Liu, *Chem. Rev.*, **111**, 3577 (2011).
6. http://www.luxresearchinc.com/news-and-events/press-releases/read/li-ion-dominates-booming-grid-storage-market-90-2014-proposals
7. U.S. Department of Energy, Grid energy storage (2013).
8. A. Z. Weber, M. M. Mench, J. P. Meyers, P. N. Ross, J. T. Gostick, and Q. Liu, *J. Appl. Electrochem.*, **41**, 1137 (2011).
9. P. Leung, X. Li, C. P. de León, L. Berlouis, C. T. J. Low, and F. C. Walsh, *RSC Adv.*, **2**, 10125 (2012).
10. W. Wang, Q. Luo, B. Li, X. Wei, L. Li, and Z. Yang, *Adv. Funct. Mater.*, **23**, 970 (2013).
11. S. Ha and K. G. Gallagher, *J. Power Sources*, **296**, 122 (2015).
12. L. Thaller, Electrically rechargeable redox flow cells. NASA-TM X-71540 (1974).
13. R. M. Darling, K. G. Gallagher, J. A. Kowalski, S. Ha, and F. R. Brushett, *Energy Environ. Sci.*, **7**, 3459 (2014).
14. J. Noack, N. Roznyatovskaya, T. Herr, and P. Fischer, *Angew. Chem. Int. Ed.*, **54**, 9776 (2015).
15. B. Schwenzer, J. Zhang, S. Kim, L. Li, J. Liu, and Z. Yang, *ChemSusChem*, **4**, 1388 (2011).
16. L. W. Hruska and R. F. Savinell, *J. Electrochem. Soc.*, **128**, 18 (1981).
17. S.-H. Shin, S.-H. Yun, and S.-H. Moon, *RSC Adv.*, **3**, 9095 (2013).
18. R. Darling, K. Gallagher, W. Xie, L. Su, and F. Brushett, *J. Electrochem. Soc.*, **163**, A5029 (2016).
19. K. A. Mauritz and R. B. Moore, *Chem. Rev.*, **104**, 4535 (2004).
20. M. Doyle, M. E. Lewittes, M. G. Roelofs, S. A. Perusich, and R. E. Lowrey, *J. Membr. Sci.*, **184**, 257 (2001).
21. Z. Tang, R. Svoboda, J. S. Lawton, D. S. Aaron, A. B. Papandrew, and T. A. Zawodzinski, *J. Electrochem. Soc.*, **160**, F1040 (2013).
22. W. Xie, J. Cook, H. B. Park, B. D. Freeman, C. H. Lee, and J. E. McGrath, *Polymer*, **52**, 2032 (2011).

23. A. Hexemer, W. Bras, J. Glossinger, E. Schaible, E. Gann, R. Kirian, A. MacDowell, M. Church, B. Rude, and H. Padmore, *J. Phys. Conf. Ser.*, **247**, 012007 (2010).
24. J. Ilavsky, *J. Appl. Crystallogr.*, **45**, 324 (2012).
25. F. Zhang, J. Ilavsky, G. G. Long, J. P. G. Quintana, A. J. Allen, and P. R. Jemian, *Metall. Mater. Trans. A*, **41**, 1151 (2009).
26. K. Kondo, M. Sano, A. Hiwara, T. Omi, M. Fujita, A. Kuwae, M. Iida, K. Mogi, and H. Yokoyama, *J. Phys. Chem. B*, **104**, 5040 (2000).
27. G. Gebel, P. Aldebert, and M. Pineri, *Polymer*, **34**, 333 (1993).
28. L. A. Zook and J. Leddy, *Anal. Chem.*, **68**, 3793 (1996).
29. F. A. L. Dullien, *Porous Media: Fluid Transport and Pore Structure*, p. 598, Academic Press, (2012).
30. K. Xu, *Chem. Rev.*, **104**, 4303 (2004).
31. Q. Duan, H. Wang, and J. Benzinger, *J. Membr. Sci.*, **392**, 88 (2012).
32. K. Schmidt-Rohr and Q. Chen, *Nat. Mater.*, **7**, 75 (2008).
33. G. Gebel and O. Diat, *Fuel Cells*, **5**, 261 (2005).
34. M. Fujimura, T. Hashimoto, and H. Kawai, *Macromolecules*, **14**, 1309 (1981).
35. H.-G. Haubold, T. Vad, H. Jungbluth, and P. Hiller, *Electrochimica Acta*, **46**, 1559 (2001).
36. K. M. Beers, D. T. Hallinan, X. Wang, J. A. Pople, and N. P. Balsara, *Macromolecules*, **44**, 8866 (2011).
37. P. Arora and Z. (John) Zhang, *Chem. Rev.*, **104**, 4419 (2004).
38. D. Novikov, S. Burlatsky, R. M. Darling, V. V. Atrazhev, V. I. Sultanov, T. Y. Astakhova, L. Su, and F. R. Brushett, submitted.
39. F. R. Brushett, J. T. Vaughey, and A. N. Jansen, *Adv. Energy Mater.*, **2**, 1390 (2012).
40. Z. Cai, Y. Liu, S. Liu, L. Li, and Y. Zhang, *Energy Environ. Sci.*, **5**, 5690 (2012).
41. W. Xie, H. Ju, G. M. Geise, B. D. Freeman, J. I. Mardel, A. J. Hill, and J. E. McGrath, *Macromolecules*, **44**, 4428 (2011).
42. M. Nič, J. Jirát, B. Košata, A. Jenkins, and A. McNaught, Eds., in *IUPAC Compendium of Chemical Terminology*, IUPAC, Research Triagle Park, NC (2009).
43. W. Xie, R. M. Darling, and M. L. Perry, *J. Electrochem. Soc.*, **163**, A5084 (2016).